Journal of Materials Chemistry

Cite this: J. Mater. Chem., 2012, 22, 5065

www.rsc.org/materials

PAPER

Synergistic catalysis of Au-Co@SiO_2 nanospheres in hydrolytic dehydrogenation of ammonia borane for chemical hydrogen storage†

Zhang-Hui Lu,[a] Hai-Long Jiang,[a] Mahendra Yadav,[a] Kengo Aranishi[ab] and Qiang Xu*[abc]

Received 26th September 2011, Accepted 19th January 2012
DOI: 10.1039/c2jm14787d

Core–shell structured Au-Co@SiO_2 nanospheres have been synthesized using a reverse-micelle method. During heat treatment in vacuum, multiple Au-Co nanoparticles (NPs) embedded in SiO_2 nanospheres (Au-Co@SiO_2-RT) merged into single Au-Co NPs in SiO_2 (Au-Co@SiO_2-HT), resulting in a size increase of the Au-Co NPs. The Au-Co@SiO_2-HT nanospheres showed better catalytic activity than that of Au-Co@SiO_2-RT. The higher catalytic activity of Au-Co@SiO_2-HT could be attributed to the decrease in the content of basic ammine by the decomposition of metal ammine complexes during the heat treatment. Compared with their monometallic counterparts, the bimetallic Au-Co NPs embedded in a SiO_2 nanosphere show higher catalytic activity for the hydrolytic dehydrogenation of NH_3BH_3 to generate a stoichiometric amount of hydrogen at room temperature for chemical hydrogen storage. The synergistic effect between Au and Co inside the silica nanospheres plays an important role in the catalytic hydrolysis of NH_3BH_3.

1. Introduction

Hydrogen has attracted considerable attention as a globally accepted clean energy carrier. Currently, the search for safe and efficient hydrogen storage materials is one of the most difficult challenges for the transformation to a hydrogen-powered society as a long-term solution for a secure energy future. To meet the US Department of Energy (DOE) target for on-board applications, hydrogen storage materials must have a high gravimetric hydrogen capacity with a rapid hydrogen release rate. There have been a large number of reports on hydrogen storage materials.[1–9] However, big challenges still remain. Ammonia borane (NH_3BH_3, AB) has a hydrogen capacity as high as 19.6 wt%, exceeding that of gasoline and making it an attractive candidate for chemical hydrogen storage applications.[10–19] Intensive efforts have been made to enhance the kinetics of the hydrogen release from this compound from both solid and solution approaches.[20–27] In this laboratory, we have thus been exploring efficient and economical catalysts[24–27] and are systematically investigating cobalt-based catalysts that exhibit high efficiency for hydrogen generation.[28–31]

Nanoparticles (NPs) coated on spherical silica or within silica hollow spheres have attracted increasing attention in the fields of catalysis,[32,33] absorbents,[34,35] photonics,[36,37] and magnetics.[38] Different approaches have been developed to synthesize such materials, most of which were micrometer sized particles.[39,40] Due to the possibility of obtaining monodisperse NPs, the synthesis of ultrafine metal NPs in a reverse micelle system has received much attention.[32] Some ultrafine metal NPs within silica nanospheres have been successfully synthesized by using a crystal template method in a reverse micelle system.[34,35,41–43]

Herein, for the first time, we report the synthesis of two core–shell structured Au-Co@SiO_2-RT and Au-Co@SiO_2-HT nanospheres, of which the latter is prepared by heat treatment of the former, with small Au-Co NPs (<3 nm diameter) embedded in the SiO_2 nanospheres. Compared with monometallic Au@SiO_2 and Co@SiO_2, both of the Au-Co@SiO_2 catalysts show higher catalytic activity for the hydrolysis of ammonia borane, generating a stoichiometric amount of hydrogen. Unexpectedly, Au-Co@SiO_2-HT with relatively large single Au-Co NPs embedded in SiO_2 nanospheres presents a better catalytic activity than Au-Co@SiO_2-RT with multiple small Au-Co NPs embedded in SiO_2 nanospheres, which is due to the decrease in the content of basic ammine by the decomposition of metal ammine complexes during the heat treatment.

2. Experimental

2.1 Chemicals

Ammonia-borane (NH_3BH_3, Aviabor, 97%), sodium borohyride ($NaBH_4$, Aldrich, 99%), hexamminecobalt(III) chloride ($Co(NH_3)_6Cl_3$, Mitsuwa Chem. Co., >99.0%), hydrogen tetrachloroaurate(III) tetrahydrate ($HAuCl_4 \cdot 4H_2O$, Wako Pure

[a]National Institute of Advanced Industrial Science and Technology (AIST), Ikeda, Osaka, 563-8577, Japan
[b]Graduate School of Engineering, Kobe University, Nada Ku, Kobe, Hyogo, 657-8501, Japan
[c]CREST, Japan Science and Technology Agency (JST), Kawaguchi, Saitama, 332-0012, Japan. E-mail: q.xu@aist.go.jp
† Electronic supplementary information (ESI) available. See DOI: 10.1039/c2jm14787d

Chemical Industries, Ltd., >99%), ethylenediamine ($C_2H_8N_2$, Tokyo Kasei Kogyo Co. Ltd., >98%), diethyl ether ($C_2H_5OC_2H_5$, Kishida Chem. Co., >99.5%), ethanol (CH_3CH_2OH, Kishida Chem. Co., >99.8%), tetraethoxysilane ($Si(OC_2H_5)_4$, Kishida Chem. Co., >99.0%), polyethylene glycol mono-4-nonylphenyl ether $n \approx 5$ (NP-5, $HO(CH_2CH_2O)_nC_6H_4C_9H_{19}$, Tokyo Kasei Kogyo Co. Ltd.), ammonia solution ($NH_3 \cdot H_2O$, Wako Pure Chemical Industries, Ltd., 28%), cyclohexane (C_6H_{12}, Kishida Chem. Co., >99.5%), methanol (CH_3OH, Kishida Chem. Co., 99.8%), and acetone ($(CH_3)_2CO$, Kishida Chem. Co., >99.5%) were used as received. Deionized water with a specific resistance of 18.2 MΩ cm was obtained by reverse osmosis followed by ion-exchange and filtration (RFD 250NB, Toyo Seisakusho Kaisha, Ltd., Japan). The $Au(en_2)Cl_3$ precursor was synthesized using $HAuCl_4 \cdot 4H_2O$ and ethylenediamine according to a previous report.[44]

2.2 Catalyst preparation

The $Au@SiO_2$, $Co@SiO_2$, and $Au\text{-}Co@SiO_2$ nanospheres were prepared in a similar manner by reverse micelle techniques[34,35,41–43] (see Fig. S1†) as follows: calculated amounts of aqueous solutions of $Au(en_2)Cl_3$ and/or $Co(NH_3)_6Cl_3$ (3.6 mL) were rapidly injected into 800 mL of NP-5 (33.6 g) cyclohexane solution. The concentrations of $Au(en)_2Cl_3$ and $Co(NH_3)_6Cl_3$ (3.6 mL) were 100 and 30 mmol L^{-1}, respectively. After stirring at room temperature for about 15 h, a 28% aqueous ammonia solution (3.6 mL) was injected rapidly and after 2 h, 4.16 mL tetraethoxysilane (TEOS) was added. The gold and cobalt contents of the products (Au : (Au + Co + SiO_2) and Co : (Au + Co + SiO_2)) were theoretically determined from the concentrations of the metal ammine complexes to be 1.9 wt% in all the samples. After 2 days stirring, the resulting solution was phase separated by the addition of methanol, followed by washing with cyclohexane and acetone, and then the sample was collected by centrifugation (15 000 rpm, 5 min, 298 K). After drying in a desiccator overnight, the solids obtained were evacuated at 293 K (room temperature) for 12 h and labeled as $Au@SiO_2$-RT, $Co@SiO_2$-RT, and $Au\text{-}Co@SiO_2$-RT. Furthermore, evacuation of the resulting solids was continued at 573 K (high temperature) for 5 h and labeled as $Au@SiO_2$-HT, $Co@SiO_2$-HT, and $Au\text{-}Co@SiO_2$-HT.

2.3 Characterization

Powder X-ray diffraction (XRD) studies were performed on a Rigaku RINT-2000 X-ray diffractometer with a $Cu_{K\alpha}$ source (40 kV, 40 mA). The morphologies and sizes of all the samples were observed by using a Tecnai G^2 20 Twin transmission electron microscope (TEM) equipped with selected area electron diffraction (SAED) and an energy-dispersive X-ray detector (EDX) at an acceleration voltage of 200 kV. X-Ray photoelectron spectroscopic (XPS) analysis was carried out on a Shimadzu ESCA-3400 X-ray photoelectron spectrometer using a $Mg_{K\alpha}$ source (10 kV, 10 mA). Argon sputtering experiments were carried out under the conditions of background vacuum = 3.2×10^{-6} Pa and sputtering acceleration voltage = 1 kV. Surface area measurements were performed by dinitrogen adsorption at liquid nitrogen temperature using automatic volumetric adsorption equipment (Belsorp mini II).

2.4 Experimental procedures for the hydrolysis of ammonia borane

A mixture of sodium borohydride ($NaBH_4$, 5 mg), ammonia borane (NH_3BH_3, 25.5 mg, 97%), and catalyst (125 mg) was placed in a two-necked round-bottomed flask, which was placed in a water bath maintained at room temperature (25 °C). A burette filled with water was connected to the reaction flask to measure the volume of hydrogen. The reaction started when distilled water (5 mL) was injected into the mixture using a syringe. The volume of the evolved hydrogen gas was measured by recording the displacement of water in a gas burette. The reaction was completed when there was no more gas generation.

For testing the durability of the catalysts, after the hydrogen generation reaction was completed, another equivalent of NH_3BH_3 (25.5 mg, 97%) was subsequently added to the reaction flask and the released gas was monitored by the gas burette. Such test cycles of the catalyst for the hydrolysis of NH_3BH_3 were carried out 5 times. After the reaction, the catalysts were separated from the reaction solution by centrifugation and reused as the catalyst for the hydrolysis of NH_3BH_3.

3. Results and discussion

The as-synthesized core–shell structured nanospheres were analyzed by powder X-ray diffraction (XRD), as shown in Fig. 1.

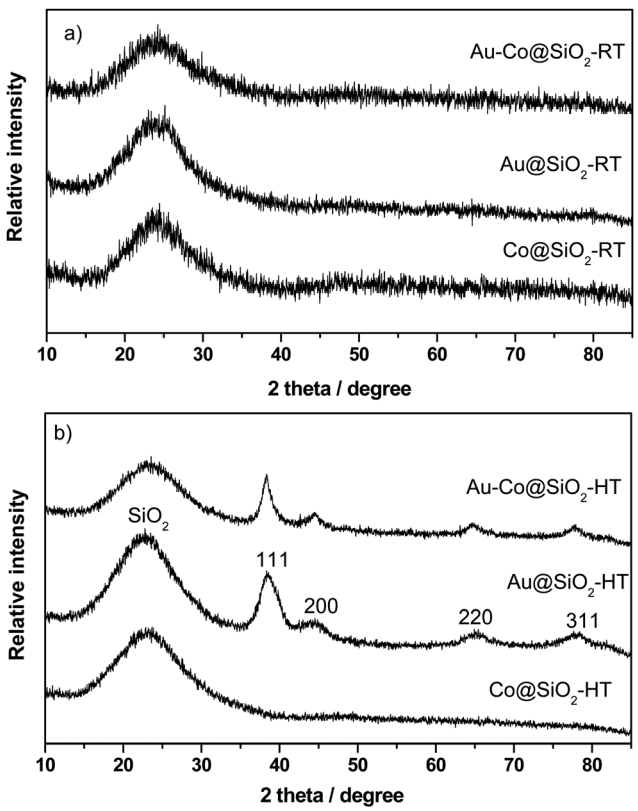

Fig. 1 Powder X-ray diffraction patterns for the as-synthesized metal-embedded SiO_2 nanospheres with a) room temperature and b) high temperature evacuation.

The strong and broad peaks in the range of $2\theta = 15–35°$ can be assigned to amorphous SiO_2 in all the samples. As for the Au@SiO_2-RT, Co@SiO_2-RT, and Au-Co@SiO_2-RT samples, there is only amorphous SiO_2, with no cobalt or gold diffractions being detected in the XRD profiles (Fig. 1a). Also, no diffractions of cobalt were detected in Co@SiO_2-HT and Au-Co@SiO_2-HT. However, for Au@SiO_2-HT and Au-Co@SiO_2-HT (Fig. 1b), four peaks that can be indexed undisputedly to cubic Au (cubic space group *Fm*3*m*, $a = 0.4078$ nm, JCPDS Card No. 04-0784) were observed in addition to the diffraction from the amorphous SiO_2 (Fig. 1b). The Au NPs in the Au@SiO_2-HT and Au-Co@SiO_2-HT nanospheres could be generated by the decomposition of metal ammine complexes during the heat treatment in vacuum.[42] The mean size of Au NPs in Au-Co@SiO_2-HT calculated from the Scherrer formula using the (111) peak is *ca.* 5.3 nm. The Co NPs were not observed from XRD in these nanospheres, which is probably because the cobalt NPs are too small and/or amorphous.

Fig. 2 shows transmission electron microscopy (TEM) images of Au-Co@SiO_2-RT (Fig. 2a–2c) and Au-Co@SiO_2-HT (Fig. 2d–2f) at different magnifications. The TEM images of the two samples reveal that the core–shell structures consist of well-proportioned spherical SiO_2 particles in which small Au-Co NPs are embedded in the center of these SiO_2 nanospheres. The nucleation and growth of metal ammine complexes in the reverse micelle is responsible for the formation of the core–shell structures (Fig. S1†). For Au-Co@SiO_2-RT, Fig. 2a–2c clearly show multiple dark spots corresponding to multiple small nanoparticles of Au-Co ammine complexes (<2 nm) in each silica nanosphere (~25 nm), confirmed by high-angle annular dark-field scanning transmission electron microscopy (HAADF–STEM) combined with energy-dispersive X-ray (EDX) spectrometry experiments (Fig. S2, ESI†). However, as shown in Fig. 2d–2f, Au-Co@SiO_2-HT exhibits only one relatively large Au-Co NP (<3 nm) in each SiO_2 nanosphere (~20 nm), supported by the HAADF–STEM and EDX experiments (Fig. S3†). The corresponding SAED patterns indicate the amorphous nature of Au-Co@SiO_2-RT and the low degree of crystalliity of Au-Co@SiO_2-HT (Fig. S4†), respectively, consistent with the XRD results. Comparing Fig. 2a–2c and Fig. 2d–2f reveals no obvious change in the spherical morphology of the silica nanospheres, but indicates that after heat treatment the size of the metal NPs inside the nanospheres increased, with a size of less than 3 nm. Previous studies have shown that the decomposition of ammine complexes took place at around 523–573 K with the evolution of decomposed gases (NH_3).[42,45] It is interesting to note that multiple nanoparticles of Au-Co ammine complexes embedded in SiO_2 nanospheres (Au-Co@SiO_2-RT) transformed into a relatively large single Au-Co NP in SiO_2 (Au-Co@SiO_2-HT) during heat treatment in vacuum, which may be due to the fact that adjacent nanoparticles can fuse together during the thermal decomposition of the metal ammine complexes. In addition, the high temperature evacuation may cause the densification of Si–O–Si bonds,[42] resulting in a decrease in the particle sizes of the SiO_2 spheres (Fig. 2c *vs.* 2f).

A nitrogen adsorption–desorption study (Fig. 3) showed that Au-Co@SiO_2-RT and Au-Co@SiO_2-HT nanospheres before hydrolysis of NH_3BH_3 have a Brunauer–Emmett–Teller (BET) surface area of 107 and 116 $m^2\ g^{-1}$, respectively. Au-Co@SiO_2-RT and Au-Co@SiO_2-HT nanospheres present similar surface areas and curve shapes. The type II isotherms with a small hysteresis loop occur at a relative pressure of 0.8–1.0 (Fig. 3), showing the existence of mesopores and/or macropores, which is probably due to void spaces formed by the stacking of nanospheres in the SiO_2 nanospheres.

The catalytic activity of the as-synthesized nanospheres towards the hydrolytic dehydrogenation of NH_3BH_3 was evaluated in a typical water-filled burette system. Fig. 4 and 5 show the time course of the hydrogen generation from NH_3BH_3 (0.16 M, 5 mL) with $NaBH_4$ (5 mg) in the presence of the as-synthesized nanospheres. It was found that the reaction rate and the amount of hydrogen evolution significantly depend on

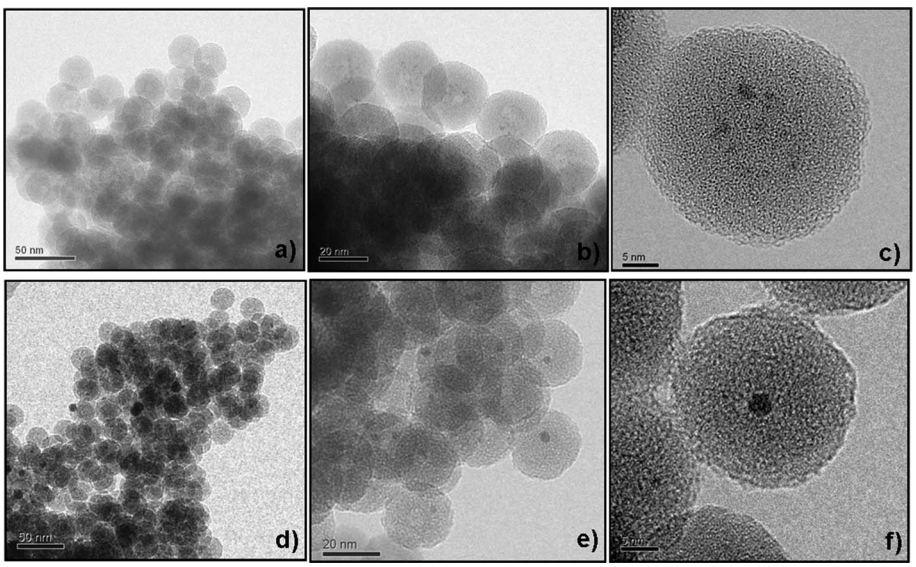

Fig. 2 Representative TEM images of the as-synthesized Au-Co@SiO_2-RT (a–c) and Au-Co@SiO_2-HT (d–f) nanospheres. Scale bars from left to right: 50, 20, 5 nm.

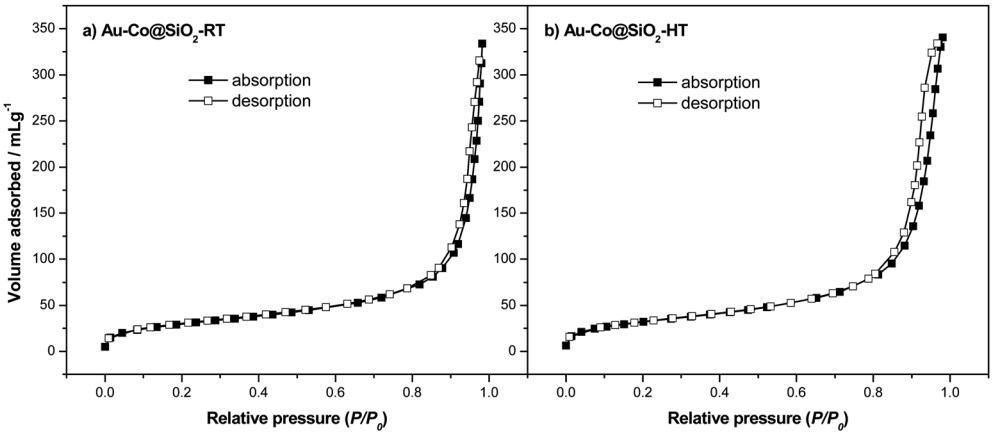

Fig. 3 Nitrogen absorption–desorption isotherms of the as-synthesized a) Au-Co@SiO_2-RT and b) Au-Co@SiO_2-HT nanospheres.

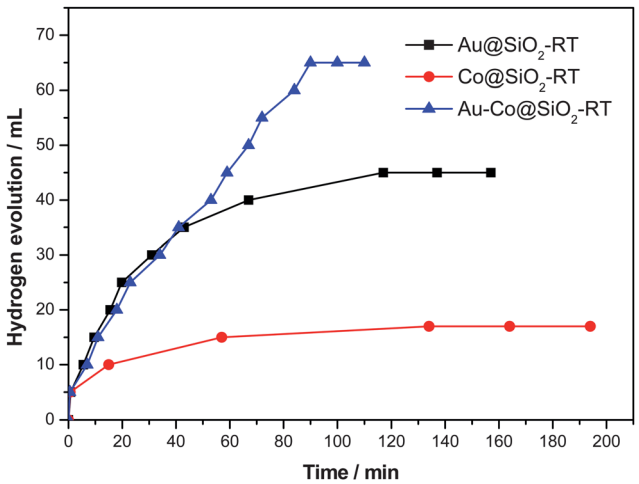

Fig. 4 Hydrogen generation from the hydrolysis of ammonia borane (AB, 0.16 M, 5 mL) with $NaBH_4$ (5 mg) in the presence of the as-synthesized Au@SiO_2-RT, Co@SiO_2-RT, and Au-Co@SiO_2-RT nanospheres (Au : AB = 0.015, Co : AB = 0.05).

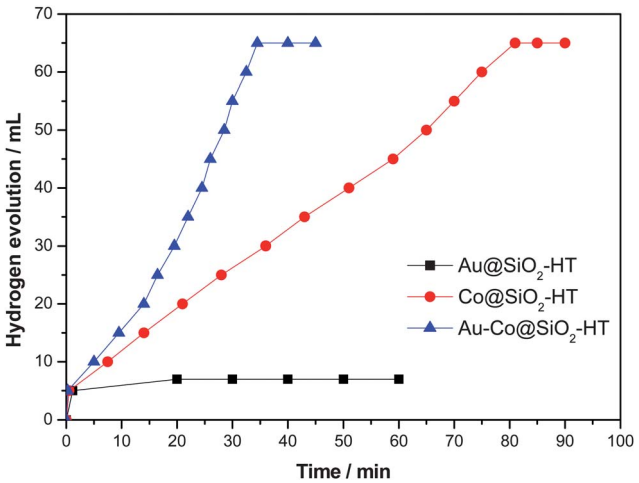

Fig. 5 Hydrogen generation from the hydrolysis of ammonia borane (AB, 0.16 M, 5 mL) with $NaBH_4$ (5 mg) in the presence of the as-synthesized Au@SiO_2-HT, Co@SiO_2-HT, and Au-Co@SiO_2-HT nanospheres (Au : AB = 0.015, Co : AB = 0.05).

the catalysts. Compared with corresponding monometallic nanospheres, both Au-Co@SiO_2-RT and Au-Co@SiO_2-HT nanospheres exhibited superior performance for the hydrolytic dehydrogenation of ammonia borane. As shown in Fig. 4 and Table S1†, the evolution of 45, 17, and 65 mL of hydrogen was completed in 117.0, 134.0, and 90.0 min, respectively, in the presence of Au@SiO_2-RT, Co@SiO_2-RT, and Au-Co@SiO_2-RT nanospheres. However, in the presence of Au@SiO_2-HT, Co@SiO_2-HT, and Au-Co@SiO_2-HT nanospheres (Fig. 5 and Table S1†), the evolution of 7, 65, and 65 mL of hydrogen was finished in 20.0, 81.0, and 34.5 min, respectively. In the present reaction system, hydrogen is generated *via* the following two reactions: $NaBH_4 + 2H_2O \rightarrow Na^+ + BO_2^- + 4H_2$ (1) and $NH_3BH_3 + 2H_2O \rightarrow NH_4^+ + BO_2^- + 3H_2$ (2). According to the theoretical calculations, the total yield of hydrogen *via* reaction 1 and reaction 2 is about 65 mL. The present experimental hydrogen productivity from NH_3BH_3 and $NaBH_4$ catalyzed by Au@SiO_2-RT, Co@SiO_2-RT, Au-Co@SiO_2-RT, Au@SiO_2-HT, Co@SiO_2-HT, and Au-Co@SiO_2-HT is around 69%, 26%, 100%, 11%, 100%, and 100% in 117.0, 134.0, 90.0, 20.0, 81.0, and 34.5 min, respectively (Table S1†). The Au-Co@SiO_2-RT, Au-Co@SiO_2-HT, and Co@SiO_2-HT nanospheres generate a stoichiometric amount of hydrogen in the hydrolysis of NH_3BH_3. It is obvious that Au-Co@SiO_2-HT presented the best activity for the generation of hydrogen, giving the highest hydrogen productivity in the shortest time amongst all the six catalysts. In addition, Au-Co@SiO_2-RT was treated at a higher temperature, 673 K, in vacuum, resulting in a sample, labeled as Au-Co@SiO_2-673 K, showing a lower activity than that of Au-Co@SiO_2-HT (Fig. S5†). In comparison with the case of the monometallic Au or Co catalyst, a high hydrogen generation rate was observed for the corresponding Au-Co bimetal embedded in silica nanospheres, suggesting that the synergetic interaction between Au and Co plays an important role in the hydrolysis of NH_3BH_3. Similar synergetic features in bimetallic NPs were found in our previous work.[8,43,46]

As shown in Fig. 6, only a negligible amount of hydrogen is generated from NH_3BH_3 with Co@SiO_2-HT catalysts in the absence of $NaBH_4$, indicating that $NaBH_4$ is necessary to

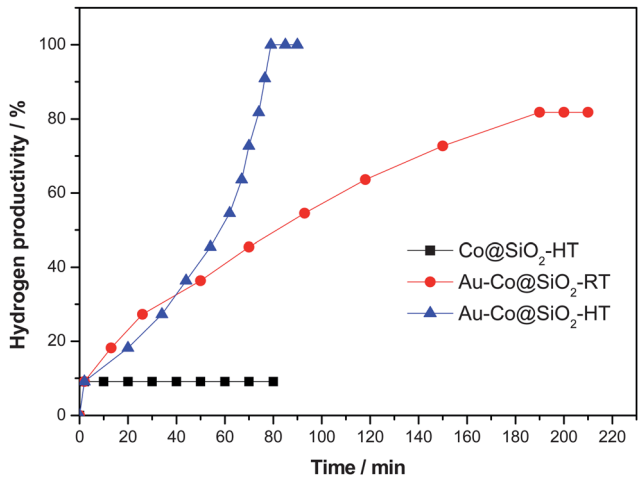

Fig. 6 Hydrogen generation by the hydrolysis of ammonia borane (AB, 0.16 M, 5 mL) without $NaBH_4$ in the presence of the as-synthesized Co@SiO_2-HT, Au-Co@SiO_2-RT, and Au-Co@SiO_2-HT nanospheres (Au : AB = 0.015, Co : AB = 0.05).

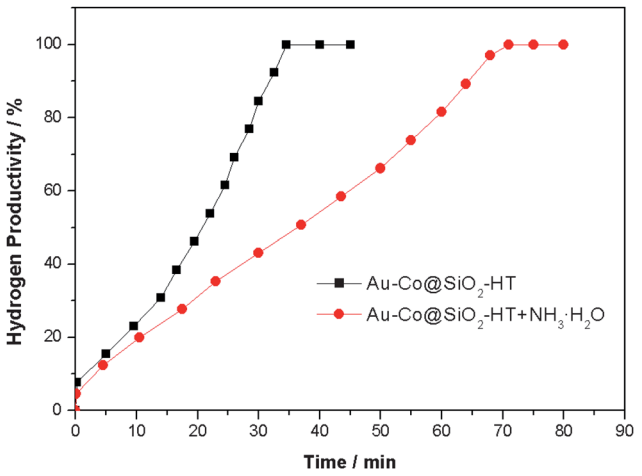

Fig. 7 Hydrogen generation from the hydrolysis of ammonia borane (AB, 0.16 M, 5 mL) with $NaBH_4$ (5 mg) in the presence of the as-synthesized Au-Co@SiO_2-HT nanospheres and Au-Co@SiO_2-HT nanospheres (Au : AB = 0.015, Co : AB = 0.05) without and with addition of ammonia solution (28%, 2 mL).

activate the catalysts. The hydrogen productivity from NH_3BH_3 without $NaBH_4$ catalyzed by Au-Co@SiO_2-RT is around 82% in 190 min. However, it is interesting to find that NH_3BH_3 can be completely converted to H_2 in 79 min without $NaBH_4$ (Fig. 6) by Au-Co@SiO_2-HT, although the activity is not as high as that in the presence of $NaBH_4$. The Au(III) can be readily reduced to Au(0) by NH_3BH_3, which has been demonstrated in a previous report.[28] However, with NH_3BH_3, it is difficult to reduce Co(II) to Co(0) due to the lower reduction potentials of Co(II)/Co(0) (reduction potentials: E^0 Co(II)/Co = −0.28 eV *vs.* SHE; E^0 Au(III)/Au = +0.93 eV *vs.* SHE). The initially formed Au NPs are catalytically active for the hydrolysis of AB and therefore might generate active intermediate Au-H species, which might facilitate the reduction of Co(II) to Co(0). These results suggest that the gold component in the catalyst not only improves the catalytic activity, but also plays a role in the activation of the catalyst.

Our previous investigations have shown that NH_3BH_3 can be hydrolyzed in the presence of solid acids and CO_2 (carbonic acid).[47] However, the present experiments showed that NH_3 (basic) had a negative effect on the catalytic reaction. As shown in Fig. 7, NH_3BH_3 can be completely converted to H_2 in 34.5 min with $NaBH_4$ by Au-Co@SiO_2-HT, whereas the reaction was finished in 71 min with addition of 2 mL $NH_3 \cdot H_2O$ (28%). The results showed that the addition of $NH_3 \cdot H_2O$ had a negative effect on the catalytic performance. Au-Co@SiO_2-HT nanospheres showed better catalytic activity than that of Au-Co@SiO_2-RT (Fig. 4–6), which could be attributed to the decrease of the NH_3 content inside the SiO_2 nanospheres during the thermal decomposition of the metal ammine complexes.

Stability or durability is very important for the practical application of catalysts. In this sense, the durability of the best catalyst, Au-Co@SiO_2-HT nanospheres, was tested in air at room temperature. As shown in Fig. 8, even after 5 runs, the productivity of hydrogen remained almost unchanged, indicating that Au-Co@SiO_2-HT nanospheres showed good durability in aqueous solution under ambient atmosphere. Furthermore, after 5 cycles of the reaction, the samples can be readily recycled by centrifugation and reused with no obvious loss of activity (Fig. S6†).

After catalytic reaction, Au-Co@SiO_2-RT and Au-Co@SiO_2-HT nanospheres still presented similar surface areas (111 $m^2\ g^{-1}$ and 109 $m^2\ g^{-1}$, respectively) and similar curve shapes to those before the catalytic reaction (Fig. S7†). No PXRD diffractions were detected for cobalt NPs in Co@SiO_2-RT after the catalytic reaction (Fig. S8†). For Au@SiO_2-RT and Au-Co@SiO_2-RT, besides the broad diffraction of amorphous SiO_2, the diffractions of Au NPs were clearly detected after catalytic reaction, which indicates that the cores were reduced to metallic NPs. For the Co@SiO_2-HT, Au@SiO_2-HT and Au-Co@SiO_2-HT nanospheres, similar PXRD results were observed before and after catalytic reaction (Fig. S8† *vs.* Fig. 1). TEM measurements were performed on the Au-Co@SiO_2-RT and Au-Co@SiO_2-HT nansopheres after catalytic reaction (Fig. 9). Comparing Fig. 2

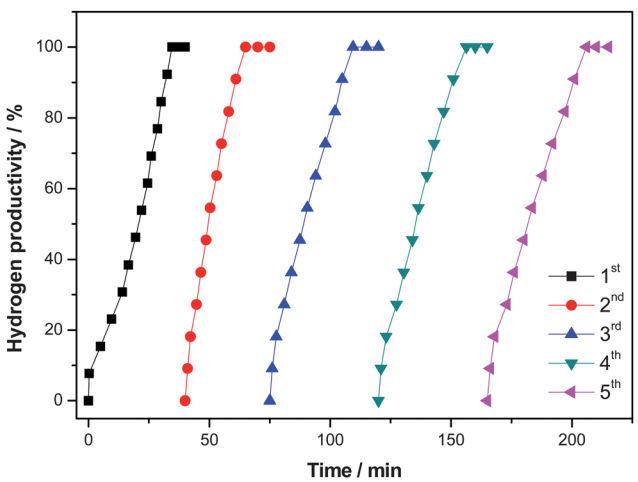

Fig. 8 Hydrogen productivity *vs.* reaction time for the generation of hydrogen from an aqueous ammonia borane solution (AB, 0.16 M, 5 mL) catalyzed by the as-synthesized Au-Co@SiO_2-HT catalysts at sequential runs by the addition of equivalent amounts of AB.

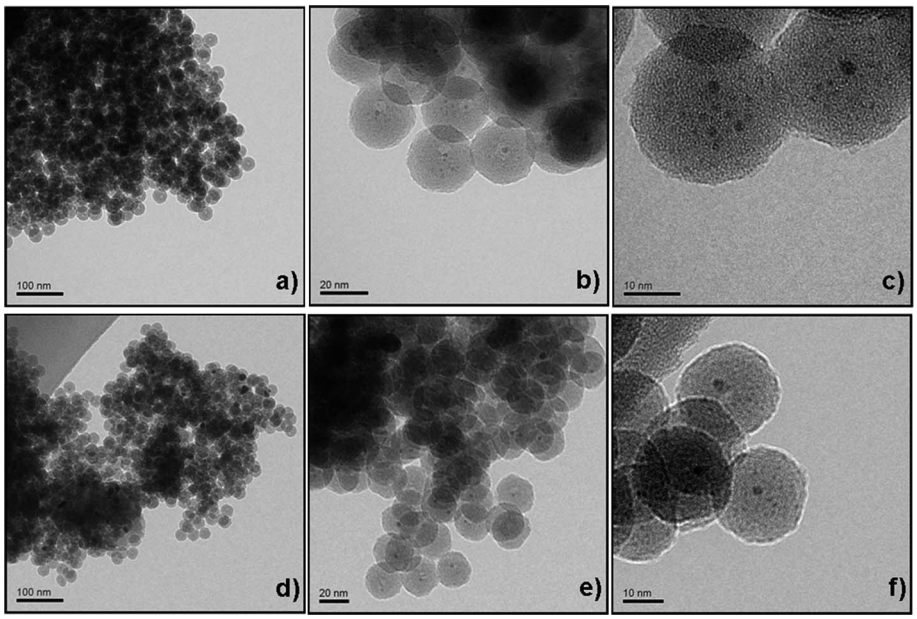

Fig. 9 Representative TEM images of the Au-Co@SiO_2-RT (a–c) and Au-Co@SiO_2-HT (d–f) nanospheres after the hydrolysis of NH_3BH_3. Scale bars from left to right: 100, 20, 10 nm.

and Fig. 9 reveals no obvious changes in the spherical morphology of the silica nanospheres for Au-Co@SiO_2-RT and Au-Co@SiO_2-HT before and after catalytic reaction. The size of the Au-Co NPs located inside SiO_2 spheres also almost remains constant after catalytic reaction. For the Au-Co@SiO_2-RT and Au-Co@SiO_2-HT nanospheres, similar HAADF–STEM, EDX, and XPS results were also obtained before and after catalytic reaction (Fig. S9–S13†). These results showed that the protection of catalytically active species inside SiO_2 nanospheres could be an effective approach for preparing catalysts with high durability.

4. Conclusions

We have successfully prepared core–shell structured Au-Co@SiO_2 nanospheres by using a metal ammine crystal template in a NP-5/cyclohexane reverse micelle system. After heat treatment in vacuum, multiple nanoparticles of Au-Co ammine complexes embedded in SiO_2 nanospheres (Au-Co@SiO_2-RT) transformed to single Au-Co NPs in SiO_2 (Au-Co@SiO_2-HT), resulting in a size increase of Au-Co NPs. Au-Co@SiO_2-HT nanospheres presented a better catalytic activity than Au-Co@SiO_2-RT nanospheres, which is attributed to the decrease in the NH_3 content during the thermal decomposition of metal ammine complexes. Compared with monometallic counterparts, Au-Co@SiO_2 nanospheres exhibit superior performance for the hydrolytic dehydrogenation of ammonia borane. These findings are encouraging and could be extended to other systems, which are used for optical, magnetic, and electrical materials as well as heterogeneous catalysts.

Acknowledgements

The authors thank the reviewers for their valuable suggestions and comments. This work was supported by AIST and JST.

References

1 U. B. Demirci and P. Miele, *Energy Environ. Sci.*, 2011, **4**, 3334–3341.
2 T. F. Hung, H. C. Kuo, C. W. Tsai, H. M. Chen, R. S. Liu, B. J. Weng and J. F. Lee, *J. Mater. Chem.*, 2011, **21**, 11754–11759.
3 P. Chen, Z. T. Xiong, J. Z. Luo, J. Y. Lin and K. L. Tan, *Nature*, 2002, **420**, 302–304.
4 N. L. Rosi, J. Eckert, M. Eddaoudi, D. T. Vodak, J. Kim, M. O'Keeffe and O. M. Yaghi, *Science*, 2003, **300**, 1127–1129.
5 X. J. Gu, Z. H. Lu and Q. Xu, *Chem. Commun.*, 2010, **46**, 7400–7402.
6 G. A. Deluga, J. R. Salge, L. D. Schmidt and X. E. Verykios, *Science*, 2004, **303**, 993–997.
7 P. Makowski, A. Thomas, P. Kuhn and F. Goettman, *Energy Environ. Sci.*, 2009, **2**, 480–490.
8 X. J. Gu, Z. H. Lu, H. L. Jiang, T. Akita and Q. Xu, *J. Am. Chem. Soc.*, 2011, **133**, 11822–11825.
9 S. W. Ting, S. Cheng, K. Y. Tsang, N. Van der Laak and K. Y. Chan, *Chem. Commun.*, 2009, 7333–7335.
10 A. Gutowska, L. Y. Li, Y. S. Shin, C. Wang, X. Li, J. C. Linehan, R. S. Smith, B. D. Kay, B. Schmid, W. Shaw, M. Gutowski and T. Autrey, *Angew. Chem., Int. Ed.*, 2005, **44**, 3578–3582.
11 M. Chandra and Q. Xu, *J. Power Sources*, 2006, **156**, 190–194.
12 M. E. Bluhm, M. G. Bradley, R. Butterick III, U. Kusari and L. G. Sneddon, *J. Am. Chem. Soc.*, 2006, **128**, 7748–7749.
13 M. C. Denney, V. Pons, T. J. Hebden, D. M. Heinekey and K. I. Goldberg, *J. Am. Chem. Soc.*, 2006, **128**, 12048–12049.
14 A. C. Stowe, W. J. Shaw, J. C. Linehan, B. Schmid and T. Autrey, *Phys. Chem. Chem. Phys.*, 2007, **9**, 1831–1836.
15 R. J. Keaton, J. M. Blacquiere and T. R. Baker, *J. Am. Chem. Soc.*, 2007, **129**, 1844–1845.
16 Z. T. Xiong, C. K. Yong, G. Wu, P. Chen, W. Shaw, A. Karkamkar, T. Autrey, M. O. Jones, S. R. Johnson, P. P. Edwards and W. I. F. David, *Nat. Mater.*, 2008, **7**, 138–141.
17 S. B. Kalidindi, M. Indiran and B. R. Jagirdar, *Inorg. Chem.*, 2008, **47**, 7424–7429.
18 S. B. Kalidindi, U. Sanyal and B. R. Jagirdar, *Phys. Chem. Chem. Phys.*, 2008, **10**, 5870–5874.
19 S. K. Kim, W. S. Han, T. J. Kim, T. Y. Kim, S. W. Nam, M. Mitoraj, L. Piekos, A. Michalak, S. J. Hwang and S. O. Kang, *J. Am. Chem. Soc.*, 2010, **132**, 9954–9955.
20 C. W. Hamilton, R. T. Baker, A. Staubitz and I. Manners, *Chem. Soc. Rev.*, 2009, **38**, 279–293.
21 U. B. Demirci and P. Miele, *Energy Environ. Sci.*, 2009, **2**, 627–637.

22 A. Staubitz, A. P. M. Robertson and L. Manners, *Chem. Rev.*, 2010, **110**, 4079–4124.
23 Y. S. Chua, P. Chen, G. T. Wu and Z. T. Xiong, *Chem. Commun.*, 2011, **47**, 5116–5129.
24 Q. Xu and M. Chandra, *J. Alloys Compd.*, 2007, **446–447**, 729–732.
25 T. Umegaki, J. M. Yan, X. B. Zhang, H. Shioyama, N. Kuriyama and Q. Xu, *Int. J. Hydrogen Energy*, 2009, **34**, 2303–2311.
26 H. L. Jiang, S. K. Singh, J. M. Yan, X. B. Zhang and Q. Xu, *ChemSusChem*, 2010, **3**, 541–549.
27 H. L. Jiang and Q. Xu, *Catal. Today*, 2010, **170**, 56–63.
28 J. M. Yan, X. B. Zhang, T. Akita, M. Haruta and Q. Xu, *J. Am. Chem. Soc.*, 2010, **132**, 5326–5327.
29 J. M. Yan, X. B. Zhang, H. Shioyama and Q. Xu, *J. Power Sources*, 2010, **195**, 1091–1094.
30 T. Umegaki, J. M. Yan, X. B. Zhang, H. Shioyama, N. Kuriyama and Q. Xu, *J. Power Sources*, 2010, **195**, 8209–8214.
31 Q. Xu and M. Chandra, *J. Power Sources*, 2006, **163**, 364–370.
32 A. J. Zarur and J. Y. Ying, *Nature*, 2000, **403**, 65–67.
33 S. Takenaka, H. Umebayashi, E. Tanabe, H. Matsune and M. Kishida, *J. Catal.*, 2007, **245**, 392–400.
34 T. Miyao, K. Minoshima and S. Naito, *J. Mater. Chem.*, 2005, **15**, 2268–2270.
35 T. Miyao, K. Minoshima, Y. Kurokawa, K. Shinohara, W. Shen and S. Naito, *Catal. Today*, 2008, **132**, 132–137.
36 M. Giersig, T. Ung, L. M. Liz-Marzan and P. Mulvaney, *Adv. Mater.*, 1997, **9**, 570–575.
37 P. Yang, Z. M. Yuan, J. Yang, A. Y. Zhang, Y. Q. Cao, Q. H. Jiang, R. X. Shi, F. T. Liu and X. Cheng, *CrystEngComm*, 2011, **13**, 1814–1820.
38 T. Haeiwa, K. Segawa and K. Konishi, *J. Magn. Magn. Mater.*, 2007, **310**, e809–e811.
39 W. Li, X. Sha, W. Dong and Z. Wang, *Chem. Commun.*, 2002, 2434–2435.
40 C. E. Fowler, D. Khushalani and S. Mann, *J. Mater. Chem.*, 2001, **11**, 1968–1971.
41 T. Miyao, N. Toyoizumi, S. Okuda, Y. Iami, K. Tajima and S. Natio, *Chem. Lett.*, 1999, 1125–1126.
42 S. Natio, K. Minoshima and T. Miyao, *Top. Catal.*, 2006, **39**, 131–136.
43 H. L. Jiang, T. Umegaki, T. Akita, X. B. Zhang, M. Haruta and Q. Xu, *Chem.–Eur. J.*, 2010, **16**, 3132–3137.
44 B. P. Block and J. C. Bailar, *J. Am. Chem. Soc.*, 1951, **73**, 4722–4725.
45 A. Klerke, C. H. Christensen, J. K. Norskov and T. Vegge, *J. Mater. Chem.*, 2008, **18**, 2304–2310.
46 H. L. Jiang and Q. Xu, *J. Mater. Chem.*, 2011, **21**, 13705–13725.
47 M. Chandra and Q. Xu, *J. Power Sources*, 2006, **159**, 855–860.